Korean J. Chem. Eng., 34(9), 2374-2382 (2017)
DOI: 10.1007/s11814-017-0148-4

pISSN: 0256-1115
eISSN: 1975-7220

Enhanced CO methanation over Ni-based catalyst using a support with 3D-mesopores

Hong-Xia Cao*, Jun Zhang*, Xiang-Kun Ren*, and Cheng-Long Guo,†**

*Low Carbon Energy Institute, China University of Mining and Technology, Xuzhou 221008, China
**School of Electrical and Power Engineering, China University of Mining and Technology, Xuzhou 221116, China
(*Received 9 March 2017 • accepted 24 May 2017*)

Abstract−Ni-based catalysts supported on a support with 3D-mesopores, including Ni/KIT-6(EG), Ni/KIT-6(PS) and Ni/KIT-6(DS), were prepared by adding ethylene glycol, direct synthesis and post synthesis methods, respectively, and their catalytic properties were investigated for CO methanation as one of the core technologies of synthetic natural gas production in a continuous flow fixed-bed reactor. The catalysts were characterized by N_2 adsorption-desorption, X-ray diffraction (XRD), transmission electron microscope (TEM), energy-dispersive X-ray spectroscopy (EDS), hydrogen temperature-programmed reduction (H_2-TPR), hydrogen temperature-programmed desorption (H_2-TPD) and thermal gravimetric analysis (TGA), respectively. The results showed that Ni/KIT-6(EG) exhibited the best catalytic performance with CO conversion of almost 100% and CH_4 yield of 75% at 450 °C, atmospheric pressure and 60,000 mL/g/h due to the higher dispersion of Ni species, stronger reducibility of NiO and formation of smaller Ni nanoparticles fixed into 3D-mesopores, indicating that adding ethylene glycol was effective to improve catalytic performance of Ni-based catalyst for CO methanation. Moreover, compared with Ni/Al_2O_3(EG) prepared using Al_2O_3 as a support, Ni/KIT-6(EG) showed better catalytic performance owing to the higher specific surface area, stronger reducibility of NiO and confinement effect of 3D-mesopores promoting to produce more active sites. After 60h lifetime test of Ni/KIT-6(EG) at 500 °C, atmospheric pressure and 60,000 mL/g/h, 3D-mesopores were still maintained and no obvious agglomeration of Ni nanoparticles was observed, meaning that Ni species were still well dispersed into 3D-mesopores. As a consequence, Ni/KIT-6(EG) exhibited superior catalytic performance and stability, which makes it a promising candidate for CO methanation.

Keywords: Ni-based Catalyst, CO Methanation, Support, Preparation Method, 3D-mesopores

INTRODUCTION

Synthetic natural gas (SNG) by coal gasification has received widespread attention due to growing demand for natural gas as an energy carrier with higher heating value and desire for clean utilization of coal resource [1,2]. However, CO methanation as one of the core technologies of SNG production, is a highly exothermic reaction, resulting in catalyst deactivation due to sintering and carbon deposition [3,4]. For this reason, extensive efforts have been devoted to the study of catalysts with higher catalytic performance and stability. Among the catalysts being explored, Ru- and Rh-based catalysts have exhibited excellent catalytic properties at lower operating temperature [5]. Unfortunately, the limited availability has restricted the commercial application of Ru- and Rh-based catalysts. Some researchers have also focused on the preparation of Fe- and Co-based catalysts [6,7], but they are nagged by lower CH_4 selectivity. In this case, Ni-based catalyst was considered as the most promising candidate for CO methanation due to its advantages, including lower price and superior catalytic performance [8-10].

Ni-based catalyst supported on the metallic oxides has been widely investigated for CO methanation [11-13]. Unfortunately, at higher operating temperature, these materials are prone to cause Ni nanoparticles agglomeration, lowering catalytic performance and stability [14-16]. Therefore, it is urgent that some novel materials with excellent physicochemical properties are developed as supports for CO methanation. Recently, researchers utilized mesoporous SiO_2 molecular sieves as supports of Ni-based catalyst, which have exhibited better catalytic performance and stability [17-21]. For example, Tao et al. [19] reported that SBA-15 was used as a support of Ni-based catalyst for improving catalytic performance. Moreover, Ni incorporated SBA-16 catalyst was also prepared by impregnation method, and the experimental results demonstrated that the catalyst displayed excellent catalytic performance [20]. In addition, Zhang et al. [21] prepared Ni-based catalyst supported on MCM-41 by hydrothermal synthesis method, and the results showed that a strong interaction between Ni species and MCM-41 inhibited catalyst sintering. Although promising, catalytic property of Ni-based catalyst was still nagged by a critical problem, that is, ineffective anchor of smaller Ni nanoparticles located inside the support [22]. As a novel silica material with 3D-mesopores, KIT-6 consisting of two interwoven subnetworks possesses higher specific surface area and pore volume [23-25], which is conducive to producing more active sites for enhancing catalytic performance and stability. Unfortunately, to date, studies on Ni-based catalyst using KIT-6 as a 3D-mesoporous support to promote catalytic property for CO methanation have not been reported. In addition, the preparation method has been considered as a critical factor affecting the catalytic property of Ni-based catalyst [26-28]. Lv et al. [26] pre-

†To whom correspondence should be addressed.
E-mail: clguo@cumt.edu.cn

pared Ni-based catalyst by the modification of silica support by adding ethylene glycol to decrease the decomposition temperature of impregnated nickel nitrate. It was also reported that Ni-based catalysts were prepared by direct synthesis and post synthesis methods for enhancing catalytic performance due to higher dispersion of active metal centers by enhancing the metal-support interaction [27,28]. Nonetheless, it was not fully understood the effect of preparation method on catalytic property of Ni-based catalyst supported on a 3D-mesoporous support for CO methanation.

We synthesized Ni-based catalysts using KIT-6 as a support with 3D-mesopores under various preparation methods and characterized by N_2 adsorption-desorption, X-ray diffraction (XRD), transmission electron microscope (TEM), energy-dispersive X-ray spectroscopy (EDS), hydrogen temperature-programmed reduction (H_2-TPR), hydrogen temperature-programmed desorption (H_2-TPD) and thermal gravimetric analysis (TGA), respectively. Moreover, the relationship between catalytic performance and 3D-mesopores as well as the effect of preparation method on catalytic performance of Ni-based catalyst for CO methanation were also explored in a continuous flow fixed-bed reactor.

EXPERIMENTAL

1. Catalyst Preparation

The support with 3D-mesopores was prepared using a triblock copolymer (P123) as structure directing agent according to the published literature [29]. Typically, 4 g P123 was dissolved into aqueous solution with 144 g distilled water and 6.6 mL HCl (35%), which was stirred at 35 °C for 2 h. Then, 4.9 mL 1-butanol was added and stirred for 1 h. Subsequently, 9.2 mL TEOS was dripped into and kept stirring at 35 °C for 24 h. The resulting mixture was transferred to a Teflon bottle and maintained at 100 °C for 24 h. The solid product collected by filtration was washed until the filtrate was neutral. After drying at 100 °C overnight, P123 was finally removed by calcination in air at 550 °C for 4 h to obtain the support with 3D-mesopores, which was named as KIT-6. KIT-6 was pretreated by incipient-wetness impregnation with ethylene glycol at room temperature for 1h and dried in an oven at 100 °C for 12 h. The modified KIT-6 was impregnated by aqueous solution of nickel nitrate under stirring at 60 °C for 10 h. Next, the solid product acquired by evaporating water under stirring at 60 °C, was dried at 100 °C overnight and calcinated in air at 550 °C for 4 h. The obtained catalyst was denoted as Ni/KIT-6(EG). For comparison, Ni-based catalyst was prepared by the same procedure with a support of Al_2O_3 instead of KIT-6, which was named as Ni/Al_2O_3(EG). KIT-6 was also added into a solution by dissolving nickel nitrate and urea with a mole ratio of 3 : 1 in 10 mL distilled water, and then kept stirred at 60 °C for 2 h. The resulting mixture was poured into a Teflon bottle and hydrothermally treated at 100 °C for 6 h. After filtration and washing, the solid product acquired by drying at 100 °C overnight and calcination in air at 550 °C for 4 h, was noted as Ni/KIT-6(PS). A nickel nitrate solution and 9.2 ml TEOS were added into aqueous solution with 4 g P123, 144 g distilled water, 6.6 mL HCl (35%) and 4.9 mL 1-butanol. After stirring at 35 °C for 24 h and hydrothermal treatment at 100 °C for 24 h, the pH value of the resulting mixture was adjusted to 8.0 with ammonia (28%). After continuous hydrothermal treatment at 100 °C for 48 h, the solid product acquired by filtration, washing and drying was calcined in air at 550 °C for 4 h, which was named as Ni/KIT-6(DS). In this work, the NiO content of all Ni-based catalysts was set to 10 wt% under various preparation methods.

2. Catalyst Characterization

N_2 adsorption-desorption isotherms at −196 °C were measured by a Micromeritics Tristar II 3000 analyzer. Prior to measurement, these samples were outgassed at 100 °C for 1 h and then at 300 °C for 3 h. The pore size distributions of samples were calculated by Barret-Joyner-Hallender (BJH) method according to desorption branch, and the specific surface areas of samples were derived from Brunauer-Emmett-Teller (BET) method. XRD patterns were recorded using a Rigaku D/MAX-2500 diffractometer. The wide-angle was in the range of 10° to 80° with scanning speed of 8°/min, and the low-angle in the range of 0.5° to 5° was performed at scanning speed of 1°/min. The average size of Ni nanoparticles was estimated by the Debye-Scherrer equation. H_2-TPR was investigated in a mixture of 10 vol% H_2/Ar with a gas flow of 30 mL/min using a Micromeritics AutoChem 2910 system with a thermal conductivity detector (TCD). The sample temperature was raised from room temperature to 800 °C at heating rate of 10 °C/min. H_2-TPD was also conducted on the same instrument like H_2-TPR. 100 mg catalyst was reduced in a pure H_2 flow of 30 mL/min for 2 h, and then cooled to 50 °C. After removing the physically adsorbed H_2, the temperature was raised to 800 °C at ramping rate of 10 °C in an Ar flow. The desorbed H_2 was detected by TCD. The number of Ni sites per unit mass was determined by H_2-TPD result based on the assumption of adsorption stoichiometry of H/Ni=1 : 1. Peak area of H_2-TPD profile was normalized by H_2-TPD result of a standard CuO sample. Ni species dispersion was calculated by the following equation [30,31]:

$$D(\%) = \frac{2 \times V_{ad} \times M \times SF}{m \times P \times V_m \times d_r} \times 100\% \quad (1)$$

where V_{ad} (mL) represents the chemisorbed H_2 volume under standard temperature and pressure (STP) in TPD measurement; M is the molar mass of Ni (58.69 g/mol); SF is the stoichiometric factor (the Ni/H molar ratio for chemisorption) which is seen as 1; m is the sample mass (g); P is the mass fraction of Ni in the sample; V_m is the molar volume of H_2 (22,414 mL/mol) at STP; d_r is the reduction degree of Ni species determined by H_2-TPR.

The TEM was employed to explore the morphology of sample by a Philips TECNAI G2F20 instrument, accompanied with EDS for measuring various elements. Before the measurement, the sample was dispersed ultrasonically into the ethanol and deposited on a holey carbon-supported grid. TGA was conducted by an STA449F3 (NETZSCH Corp.) under an air flow of 80 mL/min within a temperature range from room temperature to 800 °C at a ramping rate of 10 °C/min.

3. Catalytic Performance Measurement

CO methanation was carried out in a continuous flow fixed-bed reactor with 6 mm inner diameter quartz tube at atmospheric pressure, and the operating temperature was adjusted from 300 to 500 °C. Typically, 50 mg catalyst (40-60 mesh) mixed with 500 mg quartz sand (40-60 mesh) homogenously was loaded into quartz tube and reduced *in situ* at 550 °C in 50 vol% H_2/N_2 for 2 h. After

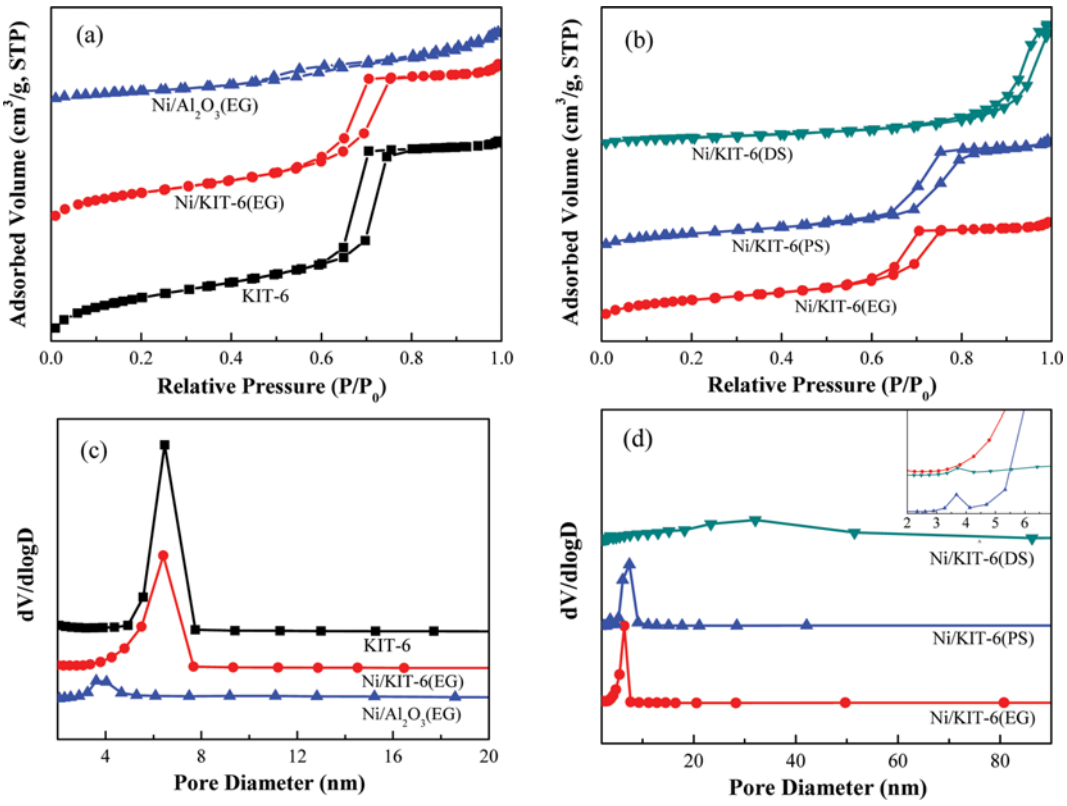

Fig. 1. N_2 adsorption-desorption isotherms of (a) KIT-6, Ni/KIT-6(EG) and Ni/Al_2O_3(EG), (b) Ni/KIT-6(EG), Ni/KIT-6(PS) and Ni/KIT-6(DS); pore size distribution curves of (c) KIT-6, Ni/KIT-6(EG) and Ni/Al_2O_3(EG), (d) Ni/KIT-6(EG), Ni/KIT-6(PS) and Ni/KIT-6(DS).

cooling to the starting operating temperature in N_2, the gas mixture composed of 60 vol% H_2, 20 vol% CO and 20 vol% N_2 was fed into the reactor at a weight hourly space velocity (WHSV) of 60,000 mL/g/h. The outlet gas was cooled and then analyzed on-line by gas chromatograph (GC-SP2100, China) with a TDX-01 and a TCD using Ar as carrier gas. In addition, the catalytic stability was performed at 500 °C and atmospheric pressure for 60 h. CO conversion, CH_4 selectivity and CH_4 yield were calculated according to the following equations:

$$\text{CO Conversion (\%)} = \frac{(V_{CO,\,in} - V_{CO,\,out})}{V_{CO,\,in}} \times 100\% \quad (2)$$

$$CH_4 \text{ Selectivity (\%)} = \frac{V_{CH_4,\,out}}{(V_{CO,\,in} - V_{CO,\,out})} \times 100\% \quad (3)$$

$$CH_4 \text{ Yield (\%)} = \frac{V_{CH_4,\,out}}{V_{CO,\,in}} \times 100\% \quad (4)$$

where $V_{i,in}$ and $V_{i,out}$ are the volume flow rate of component i (CO, CH_4) at the inlet and outlet, respectively.

RESULTS AND DISCUSSION

1. Catalyst Characterizations

1-1. N_2 Adsorption-desorption

N_2 adsorption-desorption isotherms and pore size distribution curves of KIT-6, Ni/KIT-6(EG) and Ni/Al_2O_3(EG) are presented in Fig. 1. N_2 adsorption-desorption isotherms of KIT-6 and Ni/KIT-6(EG) were attributed to typical type IV isotherms and H1 hysteresis loop [23], meaning that large channel-like pores were formed. As shown in Fig. 2(a) and (b), large channel-like pores of KIT-6 and Ni/KIT-6(EG) were also seen from TEM images, with the average pore size of 5.84 and 5.77 nm (cf. Table 1), respectively, which further confirmed the formation of large channel-like pores. Also, N_2 adsorption-desorption isotherms of KIT-6 and Ni/KIT-6(EG) increased rapidly in the relative pressure (P/P_0) from 0.6 to 0.8 due to the capillary condensation, indicating that 3D-mesopores were still preserved after Ni deposition. However, N_2 adsorption-desorption isotherm of Ni/Al_2O_3(EG) exhibited type IV isotherm and H4 hysteresis loop [32], which had the characteristics of mesoporous material. KIT-6 and Ni/KIT-6(EG) displayed two monomodal pore size distributions, corresponding to a pore around 6.5 nm, while Ni/KIT-6(PS) and Ni/KIT-6(DS) showed two bimodal pore size distributions, corresponding to the small pore around 3.7 nm/3.7 nm due to the introduction of Ni nanoparticles into 3D-mesopores and the large pore around 7.5 nm/30 nm, because of the partial damage of 3D-mesopores after Ni species doping into the skeletons of mesoporous silica, respectively. As shown in Table 1, the specific surface area, pore volume and average pore size of KIT-6 were 722.7 m^2/g, 1.07 cm^3/g and 5.84 nm, respectively, as well as the specific surface area and pore volume decreased significantly after Ni deposition. Noticeably, Ni/Al_2O_3(EG) with a monomodal pore size distribution possessed the lowest specific surface area of 186.8 m^2/g and pore volume of 0.36 cm^3/g, respectively. The average pore size of Ni/KIT-6(EG) was smaller than

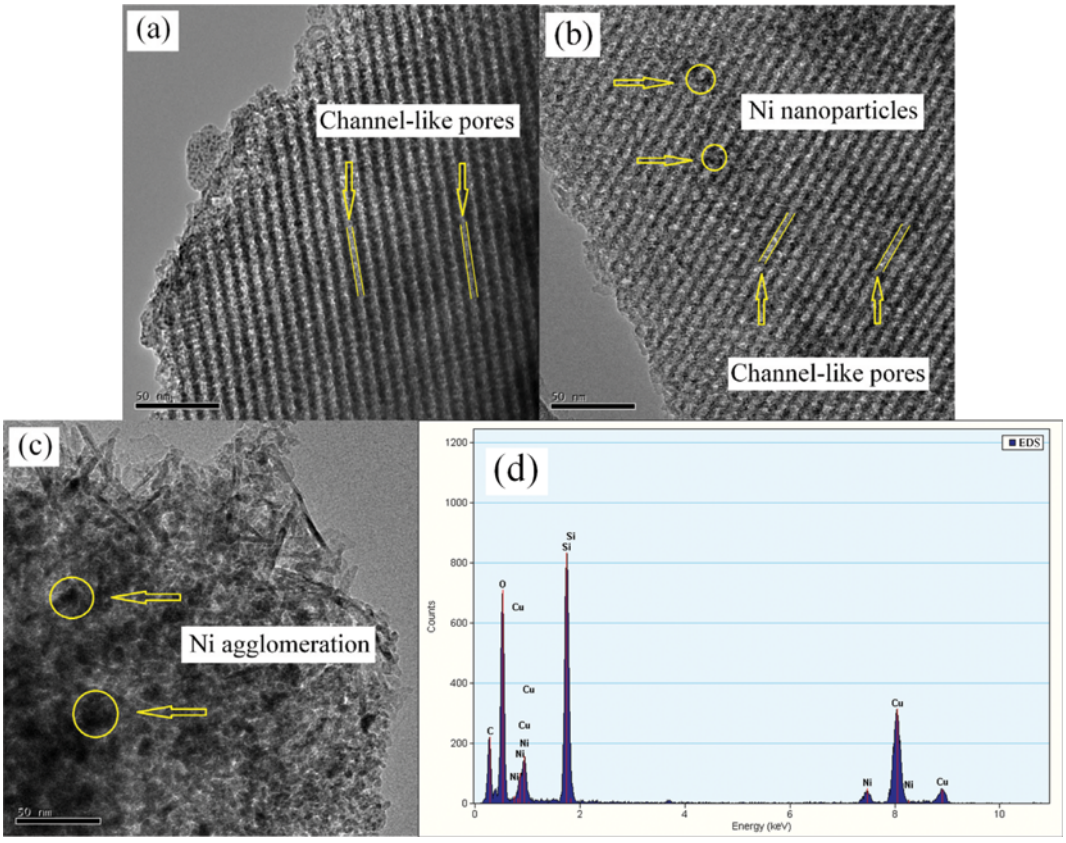

Fig. 2. TEM images of (a) KIT-6, (b) Ni/KIT-6(EG), (c) Ni/Al_2O_3(EG); (d) EDS profile of Ni/KIT-6(EG).

Table 1. Physicochemical properties of KIT-6 and catalysts

Catalyst	S_{BET} [a] (m^2/g)	V_p [b] (cm^3/g)	D_p [c] (nm)	Ni nanoparticles size (nm)		H_2 uptake (μmol/g)	D (%)[f]
				d_{Ni} [d]	d_{Ni} [e]		
KIT-6	722.7	1.07	5.84	-	-	-	-
Ni/Al_2O_3(EG)	186.8	0.36	5.76	-	6.0	93.5	13.9
Ni/KIT-6(EG)	551.3	0.86	5.77	2.4	<5	106.0	15.8
Ni/KIT-6(PS)	424.1	0.91	6.97	3.2	-	99.8	14.9
Ni/KIT-6(DS)	239.7	0.97	16.06	2.7	-	62.5	9.3

[a]Specific surface area based on the BET equation
[b]Pore volume derived from the volume of N_2 adsorbed at P/P_0=0.97
[c]Average pore size calculated by BJH method using the desorption branch
[d]Nanoparticles size estimated from Ni (111) plane using the Debye-Scherrer equation
[e]Nanoparticles size obtained from Ni (200) plane
[f]Ni species dispersion determined by the H_2-TPR and H_2-TPD

that of KIT-6, implying that Ni species were introduced into 3D-mesopores. The specific surface area of Ni/KIT-6(EG) was higher than those of Ni/KIT-6(PS) and Ni/KIT-6(DS), which is conducive to enhancing the dispersion of Ni species.

1-2. XRD Measurement

Low-angle XRD patterns of KIT-6 and Ni/KIT-6(EG) are shown in Fig. 3(a). It can be found that a sharp diffraction peak (211) was at 2θ of 0.97° and an obvious shoulder peak (220) was at 2θ of 1.10°, indicating that KIT-6 presented 3D-mesopores with cubic Ia3d space group. Meanwhile, as shown in Fig. 2(a), 3D-mesopores were observed from TEM image, which corresponded to the (211) and (220) planes in low-angle XRD pattern. Additionally, KIT-6 and Ni/KIT-6(EG) were similar in 3D-mesopores, demonstrating that 3D-mesopores were still retained after Ni deposition. Noting that, during CO methanation, 3D-mesopores were conducive to the diffusion and transfer of gas mixture as reactant, subsequently enhancing catalytic performance of Ni-based catalyst.

Fig. 3(b) displays wide-angle XRD patterns of KIT-6 and catalysts, including Ni/KIT-6(EG) and Ni/Al_2O_3(EG). For Ni/KIT-6(EG) and Ni/Al_2O_3(EG) three characteristic diffraction peaks of Ni crys-

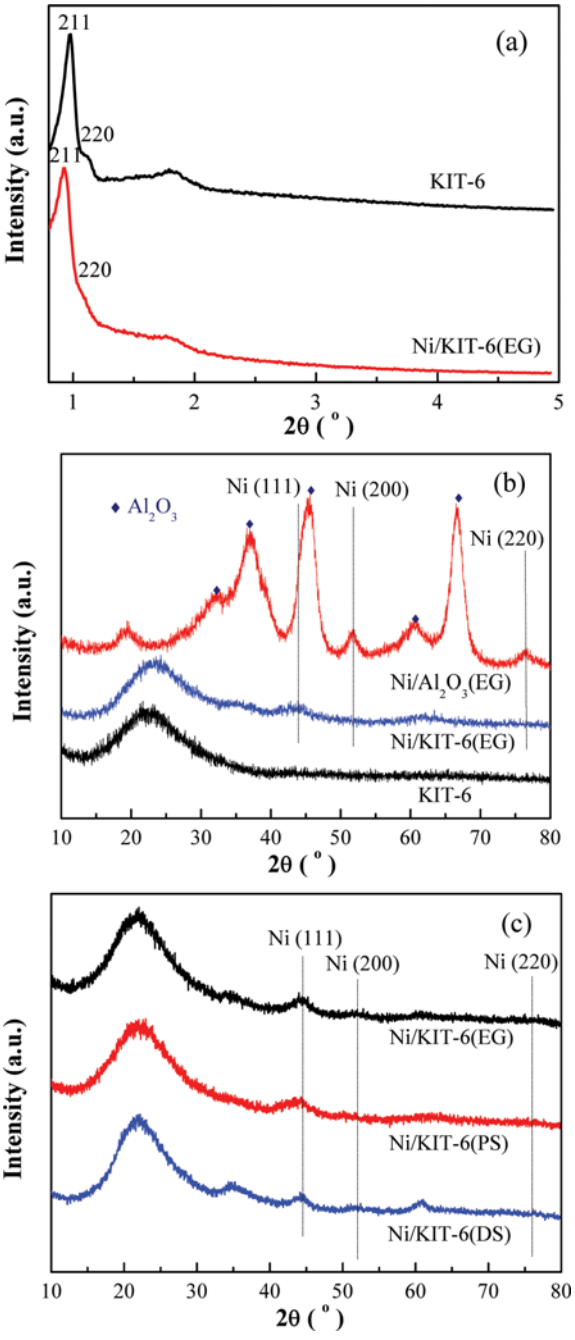

Fig. 3. (a) Low-angle XRD patterns of KIT-6 and Ni/KIT-6(EG); (b) wide-angle XRD patterns of KIT-6, Ni/KIT-6(EG) and Ni/Al_2O_3(EG); (c) wide-angle XRD patterns of Ni/KIT-6(EG), Ni/KIT-6(PS) and Ni/KIT-6(DS).

tals appeared at 2θ of 44.3°, 51.8° and 76.4°, which were, respectively, assigned to the (111), (200) and (220) planes of face-centered cubic Ni (JCPDS, No. 65-2865). For Ni/KIT-6(EG), the diffraction peak intensity from 10 to 80° was weaker than that for Ni/Al_2O_3(EG), indicating that Ni species were well dispersed on KIT-6. As seen in Fig. 2(d), EDS profile of Ni/KIT-6(EG) showed that the elements, including Ni, Si and O, were successfully introduced into 3D-mesopores, which was in line with higher dispersion of Ni species. The sizes of Ni nanoparticles estimated from XRD patterns are listed in

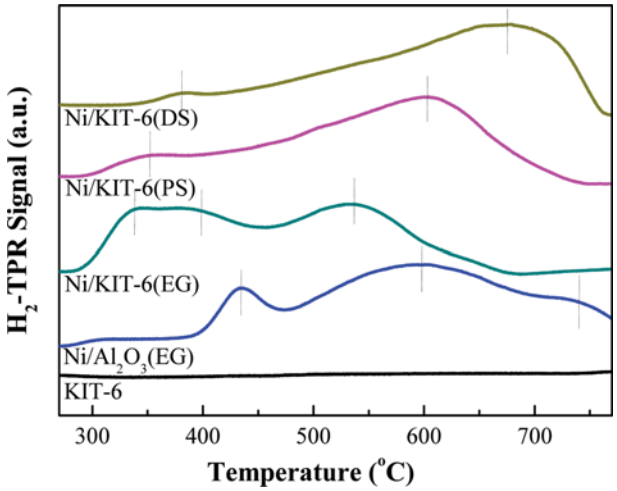

Fig. 4. H_2-TPR profiles of KIT-6, Ni/Al_2O_3(EG), Ni/KIT-6(EG), Ni/KIT-6(PS) and Ni/KIT-6(DS).

Table 1. It can be seen that the size of Ni nanoparticles dispersed on KIT-6 was smaller than that on Al_2O_3, indicating that 3D-mesopores had a significantly impact on Ni nanoparticles size, which agreed well with the results of N_2 adsorption-desorption isotherms. TEM image of Ni/KIT-6(EG) in Fig. 2(b) displayed that Ni species was evenly dispersed into 3D-mesopores, suggesting that Ni deposition cannot damage 3D-mesopores. Compared with Ni/KIT-6(EG), as shown in Fig. 2(c), Ni/Al_2O_3(EG) exhibited obvious agglomeration of Ni nanoparticles. In addition, for KIT-6 and Ni/KIT-6(EG), two broad peaks were at 2θ from 15 to 30°, implying the existence of amorphous silica.

As shown in Fig. 3(c), Ni/KIT-6(PS) and Ni/KIT-6(DS) exhibited the same characteristic diffraction peaks of Ni species as Ni/KIT-6(EG) at 2θ of 44.3°, 51.8° and 76.4°, but peak intensities were slight sharper than that of Ni/KIT-6(EG), meaning that Ni/KIT-6(EG) possessed higher dispersion of Ni species. As shown in Table 1, Ni nanoparticle size of Ni/KIT-6(EG) was smaller than those of Ni/KIT-6(PS) and Ni/KIT-6(DS). The reason was that ethylene glycol can coordinate with Ni^{2+} to disperse into 3D-mesopores and stabilize Ni element to prevent the sintering of Ni species during calcination and reduction processes, promoting the confinement effect of 3D-mesopores.

1-3. H_2-TPR Analysis

Fig. 4 presents H_2-TPR profiles of samples, including KIT-6, Ni/KIT-6(EG), Ni/Al_2O_3(EG), Ni/KIT-6(PS) and Ni/KIT-6(DS). Apparently, a reduction peak of KIT-6 cannot be observed, suggesting that all H_2 consumption peaks were assigned to NiO reduction. According to reduction peak of H_2-TPR profiles of Ni/KIT-6(EG), reducible NiO can be divided into three stages, α-, β-, and γ-stages, corresponding to low-, mid- and high-temperature peak [17]. The α-stage from 300 to 360 °C was attributed to the reduction of NiO interacting weakly with KIT-6. The β-stage around 400 °C was assigned to the reduction of bulk NiO, indicating stronger interaction between Ni species and KIT-6. The γ-stage around 540 °C resulted from the presence of Ni silicate and small NiO nanoparticles, which interacted strongly with KIT-6. Also, the reducible behavior of catalyst was remarkably affected by support material

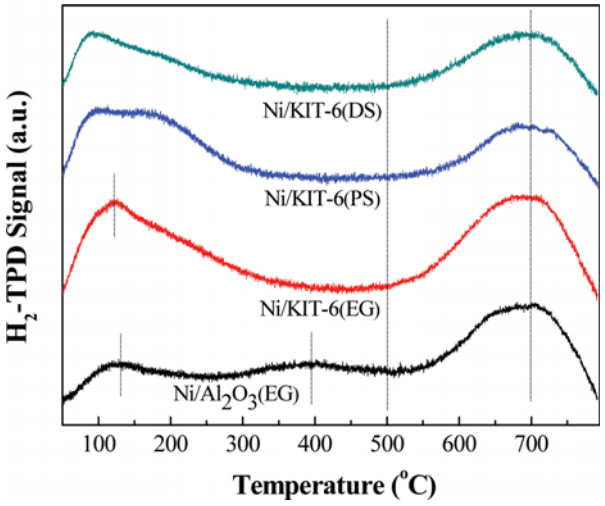

Fig. 5. H_2-TPD profiles of Ni/KIT-6(EG), Ni/Al_2O_3(EG), Ni/KIT-6(PS) and Ni/KIT-6(DS).

and preparation method. High-temperature peak of Ni/KIT-6(EG) was lower than those of other catalysts, which suggests that weakening interaction between Ni species and KIT-6 facilitated the reducibility of NiO. Compared with Ni/KIT-6(EG), high-temperature peak of Ni/Al_2O_3(EG) displayed a shift to higher temperature corresponding to stronger interaction between Ni species and Al_2O_3, which seems to be contradictory to the formation of larger Ni nanoparticles on Al_2O_3 (cf. Table 1). In fact, the confinement effect of 3D-mesopores played a key role in the formation of Ni nanoparticles, which controlled Ni nanoparticles size by limiting them in fixed space. Interestingly, reduction peaks of Ni/KIT-6(PS) and Ni/KIT-6(DS) exhibited similar trend that the intensities of low-temperature peaks decreased sharply and the intensities of high-temperature peaks rose significantly, implying the formation of small Ni nanoparticles because of the strong interaction between Ni species and KIT-6. However, Ni nanoparticle sizes of Ni/KIT-6(PS) and Ni/KIT-6(DS) were still larger than that of Ni/KIT-6(EG) (see Table 1). This was because adding ethylene glycol facilitated the immobilization of Ni^{2+} into 3D-mesopores, which contributed to the formation of smaller Ni nanoparticles by preventing the sintering of Ni species during calcination and reduction processes.

1-4. H_2-TPD Analysis

H_2-TPD profiles of Ni/KIT-6(EG), Ni/Al_2O_3(EG), Ni/KIT-6(PS) and Ni/KIT-6(DS) are presented in Fig. 5. Clearly, two H_2 desorption peaks can be observed for all catalysts, which correspond to low-temperature peaks at less than 500 °C and high-temperature peaks around 700 °C, respectively. Low-temperature peaks arose from the desorption of H_2 weakly adsorbed on Ni nanoparticles with defects. High-temperature peaks were ascribed to the desorption of strongly adsorbed H_2 and spillovered H_2, whose intensities and positions were almost no change for all catalysts. For Ni/Al_2O_3(EG), low-temperature peaks located at 131 °C and 395 °C, while that of Ni/KIT-6(EG) was shifted to lower temperature (122 °C) with only one peak, indicating higher Ni species dispersion. By comparison with Ni/KIT-6(EG), Ni/KIT-6(PS) and Ni/KIT-6(DS) exhibited two weaker peaks at lower temperature because Ni species dispersion were negatively affected by lower specific surface area and larger

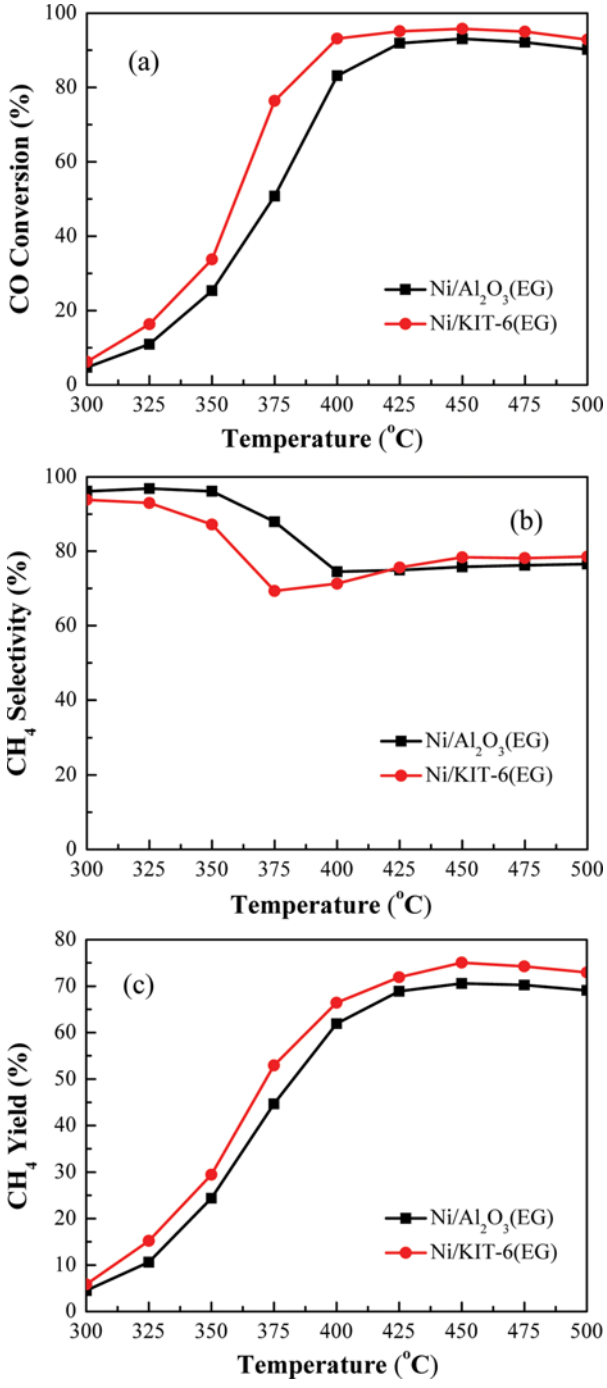

Fig. 6. Catalytic performances for CO methanation: (a) CO conversion, (b) CH_4 selectivity and (c) CH_4 yield.

Ni nanoparticles. As shown in Table 1, among all catalysts, Ni/KIT-6(EG) possessed the highest H_2 uptake of 106.0 μmol/g and Ni species dispersion of 15.8%. The result was related to higher specific surface area and effective confinement effect of 3D-mesopores, coinciding with the results from the BET measurement and TEM analysis.

2. Catalytic Performance

2-1. CO Methanation

Catalytic performance of Ni/KIT-6(EG) and Ni/Al_2O_3(EG) from

300 to 500 °C was evaluated at atmospheric pressure and a WHSV of 60,000 mL/g/h, and the results are shown in Fig. 6. Note that CO conversions of Ni/KIT-6(EG) and Ni/Al_2O_3(EG) increased first at lower operating temperature owing to the kinetics factors, and then declined at higher operating temperature due to the thermodynamic equilibrium limitation. Clearly, CH_4 selectivities of Ni/KIT-6(EG) and Ni/Al_2O_3(EG) decreased with the increase of operating temperature below 400 °C. Above 400 °C, CH_4 selectivity of Ni/Al_2O_3(EG) remained constant, while CH_4 selectivity of Ni/KIT-6(EG) showed a rising trend, suggesting that KIT-6 with 3D-mesopores had a positive impact on CH_4 selectivity. However, the produced CO_2 as by-product induced that CH_4 selectivity of Ni/KIT-6(EG) was less than 100% due to some side reactions, such as water-gas shift ($CO+H_2O \rightarrow CO_2+H_2$), Boudouard reaction ($2CO \rightarrow CO_2+C$) and reversed CH_4 and CO_2 reforming ($2CO+2H_2 \rightarrow CO_2+CH_4$). Interestingly, CO conversion and CH_4 yield of Ni/KIT-6(EG) were obviously higher than those of Ni/Al_2O_3(EG) at whole operating temperature, meaning that Ni/KIT-6(EG) possessed excellent catalytic performance. Therefore, it can be concluded that KIT-6 used as support had the higher specific surface area, stronger reducibility of NiO and confinement effect of 3D-mesopores, which facilitated to form smaller Ni nanoparticles with higher dispersion, producing more active sites and subsequently enhancing catalytic performance for CO methanation.

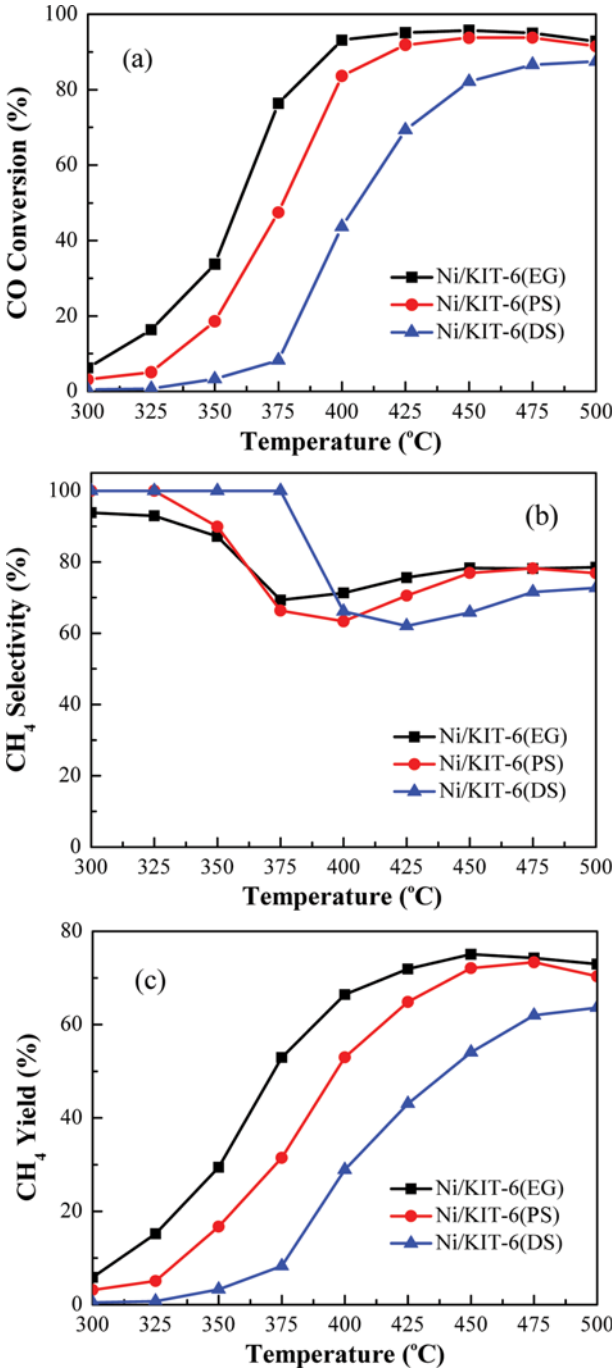

Fig. 7. Effect of preparation method on catalytic performances: (a) CO conversion, (b) CH_4 selectivity and (c) CH_4 yield.

2-2. Effect of Preparation Method

In this section, the catalytic performance of three catalysts prepared by different preparation methods, including Ni/KIT-6(EG), Ni/KIT-6(PS) and Ni/KIT-6(DS), was experimentally investigated for CO methanation, respectively. As shown in Fig. 7, among the three catalysts, Ni/KIT-6(EG) exhibited the best catalytic performance, and its CO conversion and CH_4 yield at only 450 °C reached almost 100% and 75%, respectively, while Ni/KIT-6(DS) displayed the lowest catalytic performance with 87% CO conversion and 63% CH_4 yield at 500 °C. Note that the catalytic performance of Ni/KIT-6(PS) was higher than that of Ni/KIT-6(DS), but still lower than that of Ni/KIT-6(EG). In conclusion, adding ethylene glycol was effective to improve catalytic performance of Ni-based catalyst using KIT-6 with 3D-mesopores as support for CO methanation due to the higher dispersion of Ni species, stronger reducibility of NiO and the formation of smaller Ni nanoparticles fixed into 3D-mesopores with enhanced confinement effect.

3. Catalytic Stability

Ni-based catalyst easily suffered from sintering and carbon deposition under higher operating temperature, leading to a dramatic decrease of catalytic stability [33]. Therefore, it is essential to perform a lifetime test for acquiring the catalyst with excellent catalytic stability for CO methanation. In this work, catalytic stability of Ni/KIT-6(EG) was conducted at operating temperature of 500 °C and atmospheric pressure with a WHSV of 60,000 mL/g/h for 60 h;

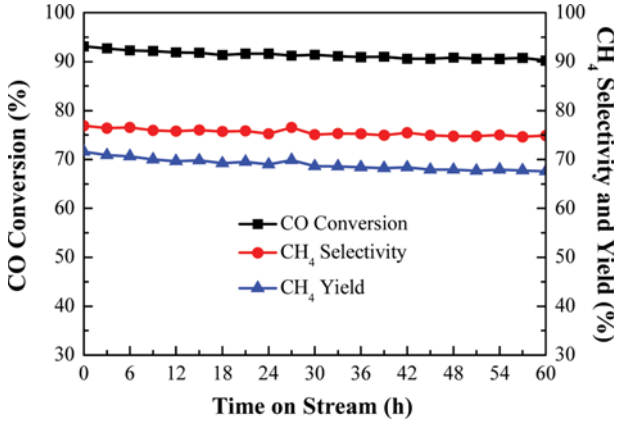

Fig. 8. 60 h lifetime test of Ni/KIT-6(EG).

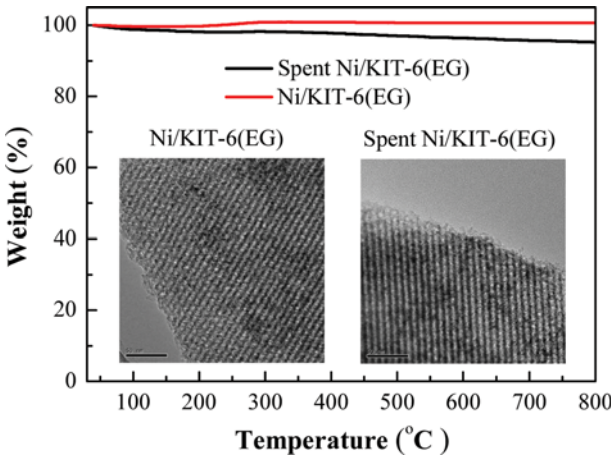

Fig. 9. TEM images and TGA profiles of Ni/KIT-6(EG) and spent Ni/KIT-6(EG) after 60 h lifetime test.

the results are displayed in Fig. 8. It cannot be seen that the obvious decreases of CO conversion, CH_4 selectivity and CH_4 yield, indicating that Ni/KIT-6(EG) had better thermal stability. This was because a large number of Ni nanoparticles were introduced into 3D-mesopores and anchored inside KIT-6, which effectively prevented the sintering of Ni species and carbon deposition on Ni nanoparticles surface, promoting catalytic stability of Ni-based catalyst. As seen from TEM image of spent Ni/KIT-6(EG) in Fig. 9, Ni nanoparticles with the size of around 3-5 nm were anchored into 3D-mesopores, which were slightly larger than that of the corresponding Ni/KIT-6(EG), but still being quite fine Ni nanoparticles. Moreover, no agglomeration of Ni nanoparticles could be observed, reflecting higher dispersion of Ni species. These observations were regarded as an indication of better anti-sintering property of Ni/KIT-6(EG). Furthermore, no signal corresponding to deposited carbon was observed in TEM, suggesting that the concentration of deposited carbon was very low. In addition, from TGA profiles in Fig. 9, the amount of deposition carbon over spent Ni/KIT-6(EG) showed a slight decrease relative to that of Ni/KIT-6(EG), indicating good anti-coking property of Ni/KIT-6(EG). Therefore, Ni/KIT-6(EG) with higher catalytic stability is considered as one of the excellent catalysts for CO methanation.

CONCLUSIONS

A series of Ni-based catalysts with NiO content of 10 wt% were successfully synthesized by different preparation methods using a support with 3D-mesopores, which can be utilized for CO methanation to produce SNG. Compared to other samples, Ni/KIT-6(EG) exhibited the highest catalytic performance with almost 100% CO conversion and 75% CH_4 yield at 450 °C and atmospheric pressure with a WHSV of 60,000 mL/g/h, which agreed well with the largest H_2 uptakes of 106.0 μmol/g and the highest Ni species dispersion of 15.8%. In a 60 h lifetime test evaluated at 500 °C and atmospheric pressure with a WHSV of 60,000 mL/g/h, Ni/KIT-6(EG) showed a good resistance to sintering of Ni species and carbon deposition on Ni nanoparticles surface. The catalysts were measured by N_2 adsorption-desorption, XRD, TEM, EDS, H_2-TPR and H_2-TPD and TGA, respectively, and the results suggested that the improvement of catalytic property was assigned to the generation of more active sites, which was derived from higher dispersion of Ni species, stronger reducibility of NiO and smaller Ni nanoparticles fixed into 3D-mesopores with enhanced confinement effect. This work revealed that Ni/KIT-6(EG) is a promising candidate with excellent catalytic performance and stability for CO methanation.

ACKNOWLEDGEMENTS

The authors gratefully acknowledge financial supported by the Fundamental Research Funds for the Central Universities (No. 2015XKMS061), and sincerely appreciate Prof. Xinbin Ma from Tianjin University for his suggestion on the experiment.

REFERENCES

1. M. Götz, J. Lefebvre, F. Mörs, M. D. Koch, F. Graf, S. Bajohr, R. Reimert and T. Kolb, *Renew. Energy*, **85**, 1371 (2016).
2. J. Gao, Q. Liu, F. Gu, B. Liu, Z. Zhong and F. Su, *RSC Adv.*, **5**, 22759 (2015).
3. J. Barrientos, M. Lualdi, R. S. París, V. Montes, M. Boutonnet and S. Järås, *Appl. Catal. A*, **502**, 276 (2015).
4. M. A. Goula, N. D. Charisiou, K. N. Papageridis, A. Delimitis, E. Pachatouridou and E. F. Iliopoulou, *Int. J. Hydrogen Energy*, **40**, 9183 (2015).
5. C. Galletti, S. Specchia and V. Specchia, *Chem. Eng. J.*, **167**, 616 (2011).
6. A. L. Kustov, A. M. Frey, K. E. Larsen, T. Johannessen, J. K. Nørskov and C. H. Christensen, *Appl. Catal. A*, **320**, 98 (2007).
7. Z. Yao, X. Zhang, P. Feng, H. Yu, H. Wang and J. Yang, *Int. J. Hydrogen Energy*, **36**, 1955 (2011).
8. Q. Liu, F. N. Gu, X. P. Lu, Y. J. Liu, H. F. Li, Z. Y. Zhong, G. W. Xu and F. B. Su, *Appl. Catal. A*, **488**, 37 (2014).
9. J. Sehested, S. Dahl, J. Jacobsen and J. R. Rostrup-Nielsen, *J. Phys. Chem. B*, **109**, 2432 (2005).
10. Y. S. Mok, H. C. Kang, H. J. Lee, D. J. Koh and D. N. Shin, *Plasma Chem. Plasma P.*, **30**, 437 (2010).
11. Q. Liu, F. Gu, J. Gao, H. Li, G. Xu and F. Su, *J. Energy Chem.*, **23**, 761 (2014).
12. M. M. Zyryanova, P. V. Snytnikov, R. V. Gulyaev, Y. L. Amosov, A. I. Boronin and V. A. Sobyanin, *Chem. Eng. J.*, **238**, 189 (2014).
13. V. M. Shinde and G. Madras, *AIChE J.*, **60**, 1027 (2014).
14. X. Q. Li, D. M. Tong and C. W. Hu, *J. Energy Chem.*, **24**, 463 (2015).
15. S. L. Ma, Y. S. Tan and Y. Z. Han, *J. Nat. Gas Chem.*, **20**, 435 (2011).
16. R. P. W. J. Struis, T. J. Schildhauer, I. Czekaj, M. Janousch, S. M. A. Biollaz and C. Ludwig, *Appl. Catal. A*, **362**, 121 (2009).
17. H. D. Li, J. Ren, X. Qin, Z. F. Qin, J. Y. Lin and Z. Li, *RSC Adv.*, **5**, 96504 (2015).
18. Q. Liu, F. Gu, Z. Zhong, G. Xu and F. Su, *Korean J. Chem. Eng.*, **33**, 1599 (2016).
19. M. Tao, X. Meng, Y. H. Lv, Z. C. Bian and Z. Xin, *Fuel*, **165**, 289 (2016).
20. Z. C. Bian, X. Meng, M. Tao, Y. H. Lv and Z. Xin, *Fuel*, **179**, 193 (2016).

21. J. Y. Zhang, Z. Xin, X. Meng and M. Tao, *Fuel*, **109**, 693 (2013).
22. T. Xie, L. Y. Shi, J. P. Zhang and D. S. Zhang, *Chem. Commun.*, **50**, 7250 (2014).
23. F. Kleitz, F. Berube, R. Guillet-Nicolas, C. Yang and M. Thommes, *J. Phys. Chem. C*, **114**, 9344 (2010).
24. K. Subramaniyan and P. Arumugam, *J. Porous Mater.*, **23**, 639 (2016).
25. F. He, J. Luo and S. Liu, *Chem. Eng. J.*, **294**, 362 (2016).
26. X. Y. Lv, J. F. Chen, Y. S. Tan and Y. Zhang, *Catal. Commun.*, **20**, 6 (2012).
27. B. W. Lu and K. Kawamoto, *RSC Adv.*, **2**, 6800 (2012).
28. B. W. Lu and K. Kawamoto, *Fuel*, **103**, 699 (2013).
29. F. Kleitz, S. H. Choi and R. Ryoo, *Chem. Commun.*, **17**, 2136 (2003).
30. Q. Liu, J. Gao, M. J. Zhang, H. F. Li, F. N. Gu, G. W. Xu, Z. Y. Zhong and F. B. Su, *RSC Adv.*, **4**, 16094 (2014).
31. G. Jin, F. Gu, Q. Liu, X. Wang, L. Jia, G. Xu, Z. Y. Zhong and F. B. Su, *RSC Adv.*, **6**, 9631 (2016).
32. M. Sanchez-Cantu, L. M. Perez-Diaz, A. M. Maubert and J. S. Valente, *Catal. Today*, **150**, 332 (2010).
33. C. Guo, Y. Wu, H. Qin and J. Zhang, *Fuel Process. Technol.*, **124**, 61 (2014).